Probing the electronic structure and Au—C chemical bonding in AuC_n^- and AuC_nH^- ($n = 2, 4$, and 6) using high-resolution photoelectron spectroscopy

Iker León, Fernando Ruipérez, Jesus M. Ugalde, and Lai-Sheng Wang'

Citation: J. Chem. Phys. **145**, 064304 (2016); doi: 10.1063/1.4960440
View online: http://dx.doi.org/10.1063/1.4960440
View Table of Contents: http://aip.scitation.org/toc/jcp/145/6
Published by the American Institute of Physics

THE JOURNAL OF CHEMICAL PHYSICS **145**, 064304 (2016)

Probing the electronic structure and Au—C chemical bonding in AuC$_n^-$ and AuC$_n$H$^-$ (n = 2, 4, and 6) using high-resolution photoelectron spectroscopy

Iker León,[1,2] Fernando Ruipérez,[3] Jesus M. Ugalde,[4] and Lai-Sheng Wang[1,a]
[1]*Department of Chemistry, Brown University, Providence, Rhode Island 02912, USA*
[2]*ICFO - Institut de Ciencies Fotoniques, The Barcelona Institute of Science and Technology, 08860 Castelldefels (Barcelona), Spain*
[3]*POLYMAT, University of the Basque Country UPV/EHU, Joxe Mari Korta Center, Avda. Tolosa 72, 20018 Donostia – San Sebastián, Spain*
[4]*Kimika Fakultatea, Euskal Herriko Unibertsitatea (UPV/EHU), and Donostia International Physics Center (DIPC), P.K. 1072, 20080 Donostia, Euskadi, Spain*

(Received 21 June 2016; accepted 23 July 2016; published online 10 August 2016)

We report a joint photoelectron spectroscopy and theoretical study on AuC$_4^-$, AuC$_6^-$, and AuC$_n$H$^-$ (n = 2, 4, and 6) using high-resolution photoelectron imaging and *ab initio* calculations. The ground state of AuC$_2$H$^-$, AuC$_4$H$^-$, and AuC$_6$H$^-$ is found to be linear, while that of AuC$_4^-$ and AuC$_6^-$ is bent. All the species are found to be linear in their neutral ground states. The electron affinities (EAs) are measured to be 3.366(1) and 3.593(1) eV for AuC$_4$ and AuC$_6$, respectively. Both bending and stretching frequencies are resolved in the spectra of AuC$_4^-$ and AuC$_6^-$. High-resolution data of AuC$_n$H$^-$ reveal major vibrational progressions in the Au—C stretching and bending modes. AuC$_2$H$^-$ has a ground state stretching frequency of 445(10) cm^{-1} and a bending frequency of 260(10) cm^{-1}; AuC$_4$H$^-$ has a ground state stretching frequency of 340(10) cm^{-1}; AuC$_6$H$^-$ has a ground state stretching frequency of 260(10) cm^{-1} and a bending frequency of 55(10) cm^{-1}. The EAs are measured to be 1.475(1), 1.778(1), and 1.962(1) eV for AuC$_2$H, AuC$_4$H, and AuC$_6$H, respectively. The strength of the Au—C bond decreases as the number of carbon atoms increases. The current study provides a wealth of electronic structure information about AuC$_4^-$, AuC$_6^-$, and AuC$_n$H$^-$ (n = 2, 4, and 6) and their corresponding neutrals. *Published by AIP Publishing.* [http://dx.doi.org/10.1063/1.4960440]

I. INTRODUCTION

The strong relativistic effects[1] give gold many unique chemical properties, such as aurophilicity and propensity to form covalent bonds.[2–4] In fact, gold has been found to be analogous to H in its bonding in alloy clusters with Si and B.[5–9] In the current study, we investigate the Au/H analogy in a series of AuC$_n^-$ and AuC$_n$H$^-$ species and the Au—C bonding because of its importance in understanding homogeneous catalyses involving gold.[10–14] We have studied previously a series of Au(I)-alkynyl complexes, LAuCCH$^-$ (L=Cl, I, and CCH) using photoelectron spectroscopy (PES) and theoretical calculations.[15] We observed an unusually large Au—C stretching frequency in these complexes, leading to the surprising finding that the Au—C bond in these complexes is extremely strong with a dissociation energy of 5.01 eV in ClAuCCH$^-$. Even more surprisingly, we found that the Au—C single bond in ClAuCCH$^-$ is even stronger than the Au=C double bond in ClAu=CH$_2$ and the Au≡C triple bond in ClAu≡C,[16–21] revealing an inverse correlation between bond strength and bond orders in the series of Au—C compounds. The auxiliary ligand L is found to polarize the Au(I) center in ClAuCCH$^-$, resulting in the unusually strong Au—C bond. To understand the polarization effects and to obtain a reference to compare with the Au—C bonding in the LAuCCH$^-$ complexes, we recently studied the bonding in Au—CC$^-$.[22] The Au—C stretching frequency in AuC$_2^-$ was found to be lower than that in ClAu—CCH$^-$ and the dissociation energy of AuC$_2^-$ ($^1\Sigma^+$) → Au (^{2}S) + C$_2^-$ ($^2\Pi_u$) was calculated to be ~3.10 eV, which is significantly smaller than the 4.52 eV or 5.23 eV dissociation energies for ClAu—CCH$^-$ ($^1\Sigma^+$) → ClAu ($^1\Sigma^+$) + CCH$^-$ ($^1\Sigma^+$) or ClAu—CCH$^-$ ($^1\Sigma^+$) → ClAu$^-$ ($^2\Sigma^+$) + CCH ($^2\Sigma^+$), highlighting the importance of the auxiliary ligand (L) in influencing the Au—C bond in LAu—CCH$^-$.

The bonding in Au—CCH$^-$ would provide even better references to assess the influence of L on the Au—C bonding in LAu—CCH$^-$. Furthermore, increasing the carbon chain length will provide information about the correlation between the carbon chain length and the strength of the Au—C bonding. In the current work, we present a study on the electronic structure and chemical bonding in AuC$_n^-$ and Au—C$_n$H$^-$ and their corresponding neutrals using high-resolution PE imaging and *ab initio* calculations. High resolution PE spectra from the ground state detachment transitions of AuC$_4^-$, AuC$_6^-$, and AuC$_n$H$^-$ (n = 2, 4, and 6) are obtained for the first time, using a velocity-map imaging (VMI) system,[23] providing detailed spectroscopic data for the corresponding neutral species.

AuC$_4^-$ and AuC$_6^-$ are found to be slightly bent, while the corresponding neutral species are linear. The PE spectra

---

[a] E-mail: Lai-Sheng_Wang@brown.edu

0021-9606/2016/145(6)/064304/11/$30.00

Published by AIP Publishing.

of AuC_4^- reveal a progression in the lowest two bending modes with frequencies of 129(10) and 192(10) cm^{-1}, a stretching mode of 378(11) cm^{-1}, and an electron affinity (EA) of 3.366(1) eV for AuC_4. The PE spectra of AuC_6^- resolve two active bending modes with frequencies of 159(11) and 188(11) cm^{-1}, a stretching mode of 263(11) cm^{-1}, and an EA of 3.593(1) eV for AuC_6. The PE spectra of AuC_nH^- on the other hand are all due to linear ← linear detachment transitions, showing extensive vibrational progressions in the Au—C stretching mode. The AuC_2H^- species shows a progression in the stretching mode of 445(10) cm^{-1} together with Fermi resonances with the bending mode of 260(11) cm^{-1}.[22] The PE spectra of AuC_4H^- show a ground state stretching frequency of 340(10) cm^{-1}, while the PE spectra of AuC_6H^- resolve a ground state stretching frequency of 260(10) cm^{-1} and a bending frequency of 55(10) cm^{-1}. The EAs are measured accurately to be 1.475(1), 1.778(1), and 1.962(1) eV for AuC_2H, AuC_4H, and AuC_6H, respectively.

The Au—C bond strength in AuC_2^-, which shows the strongest bond among the studied clusters, is considerably weaker than that in ClAu—CCH⁻, showing the importance of the auxiliary ligand in the Au—C bond. It is also found that the strength of the Au—C bond decreases as the number of carbon atoms in the chain is increased because the covalent contribution of the chemical bond decreases.

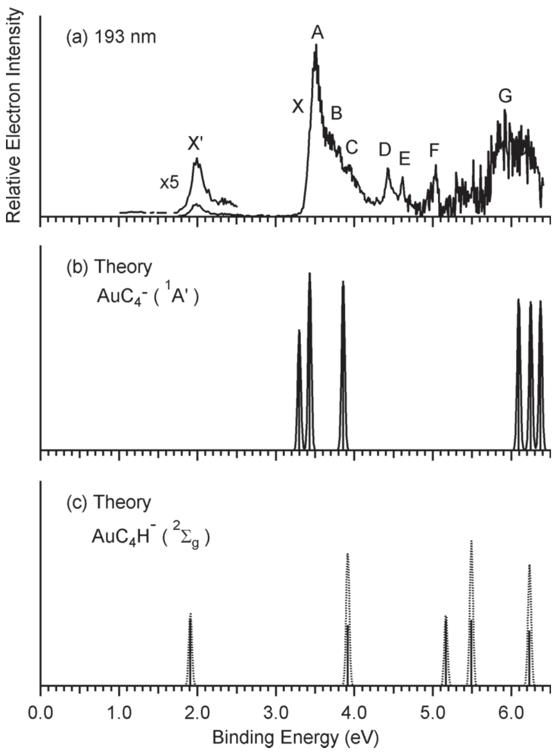

FIG. 1. (a) Photoelectron spectrum of AuC_4^- at 193 nm (6.424 eV). Simulated spectrum for (b) AuC_4^- and (c) AuC_4H^-.

II. EXPERIMENTAL AND THEORETICAL METHODS

A. Experimental methods

The experiments were done using two different PES apparatuses, which were equipped with similar laser vaporization supersonic cluster sources and time-of-flight mass spectrometry for cluster generation and size selection, but different photoelectron detections, one with a magnetic-bottle PE analyzer[24] for the high photon energy experiment at 193 nm and the other one involving a VMI system for high resolution studies.[22,23,25–27] For both experiments, a disk made of C and Au (C/Au atom ratio ∼1/9) was used as the laser vaporization target with a helium carrier gas seeded with 10% argon, which was shown to produce relatively cold gold cluster anions previously.[28] Clusters formed inside the nozzle were entrained by the carrier gas and underwent a supersonic expansion. After a skimmer, anions from the collimated cluster beam were extracted perpendicularly into a time-of-flight mass spectrometer. The AuC_n^- anions of interest were mass-selected and decelerated before being detached by a 193 nm (6.424 eV) laser beam from an ArF excimer laser in the interaction zone of the magnetic-bottle electron analyzer, which was described in detail before.[24] The AuC_nH^- species, present as impurities in the AuC_n^- beam and derived from residual contamination of

TABLE I. Relative energies (ΔE) in eV, vibrational frequencies in cm^{-1} for the low-frequency modes,[a] and bond angles for $AuC_{4,6}^-$, $AuC_{4,6}$, $AuC_{2,4,6}H^-$ and $AuC_{2,4,6}H$ calculated by CASSCF/CASPT2 including spin-orbit coupling, together with effective core potentials for Au and C. Values marked by * are calculated by DFT method using B3LYP and basis set 6-31++g(d,p) for C and Lanl2dz for Au.

	Δ E	ν_1	ν_2	ν_3	ν_4	ν_5	ν_6	α_1(deg)	α_2(deg)	α_{3-5}(deg)
Au—C_2—H^- ($^2\Sigma_g$)	0.00	339	201	615	…	…	…	…	…	180
Au—C_2—H ($^1\Sigma_g$)	1.47	485	259	686	…	…	…	…	…	180
Au—C_4^- ($^1A'$)	0.00 0.00*	372*	81*	234*	239*	520*	560*	158 153*	175 174*	180 180*
Au—C_4 ($^2\Pi$)	3.13 3.2*	339*	102*	248*	267*	577*	604*	180 180*	180 180*	180 180*
Au—C_4—H^- ($^2\Sigma_g$)	0.00	252	81	323	516	769	…	…	…	180
Au—C_4—H ($^1\Sigma_g$)	1.79	338	114	335	629	767	…	…	…	180
Au—C_6^- ($^1A'$)	0.00 0.00*	267*	57*	104*	147*	273*	323*	162 159*	177 176*	180 180*
Au—C_6 ($^2\Pi$)	3.04 3.4*	269*	59*	134*	156*	277*	286*	180 180*	180 180*	180 180*
Au—C_6—H^- ($^2\Sigma_g$)	0.00	207	41	52	140	320	337	…	…	180
Au—C_6—H ($^1\Sigma_g$)	2.02	266	63	181	347	609	712	…	…	180

[a] ν_1 - Au—C stretch; ν_2 - bending; ν_3 - bending; ν_4 - bending; ν_5 - bending; ν_6 - bending.

gold,[29] were not observable in the mass spectra due to their weak intensities and limited mass resolution. Photoelectrons were collected at nearly 100% efficiency by the magnetic bottle and analyzed in a 3.5 m long electron flight tube. The PE spectra were calibrated with the known spectrum of Bi^-. The kinetic energy resolution of the apparatus, ΔEk/Ek, was better than 2.5%, i.e., ∼25 meV for 1 eV electrons.

For the high-resolution PE imaging experiment, the AuC_n^- anions were mass-selected and focused into a collinear VMI system for photodetachment by a tunable laser.[22,23,25–27] Photoelectrons were accelerated toward a position-sensitive detector with a 75 mm diameter micro-channel plate coupled to a phosphor screen and a charge-coupled device (CCD) camera. A National Instrument PXI-mainframe system was used to control the whole apparatus and for data acquisition. The tunable radiation (222–709 nm, linewidth $<0.3\ \mathrm{cm^{-1}}$) was from a Continuum Sunlite OPO system pumped by an injection-seeded Continuum Powerlite laser. Typical pulse energies used were ∼150 μJ. A half-wave plate combined with a high-quality Glan-Laser polarizer was used to achieve a high degree of polarization parallel to the imaging detector plane. The electron count rates for the current experiment at certain wavelengths were very low, and photoelectron images were averaged with 300 000–700 000 laser shots. Inverse-Abel transformation was done to obtain the three-dimensional (3D) electron distributions from the recorded two-dimensional (2D) images. This reconstruction was done by both the BASEX[30] and pBASEX[31] programs, which yielded similar results. The imaging system was calibrated using the known spectrum of Au^-.

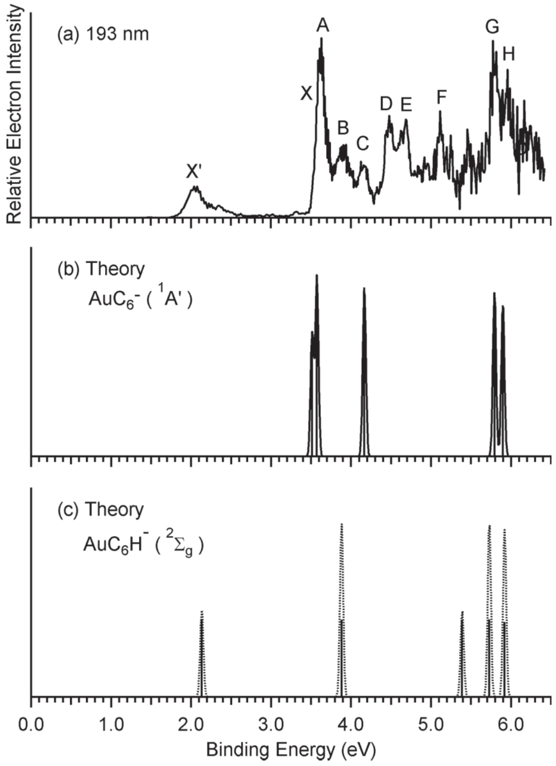

FIG. 2. (a) Photoelectron spectrum of AuC_6^- at 193 nm (6.424 eV). Simulated spectrum for (b) AuC_6^- and (c) AuC_6H^-.

B. Theoretical methods

Density Functional Theory (DFT) calculations were performed on AuC_n^- and AuC_nH^- (n = 2, 4, and 6) with the Gaussian 09 program package[32] using the B3LYP functional.[33,34] The all-electron 6-31++G(d,p) basis set[35] was used for the carbon atoms, and the Lanl2dz basis set and the associated effective core potential (ECP)[36–38] were used for gold during the optimization calculations. Vibrational frequencies were calculated to confirm that the obtained structures were true minima. In addition, wavefunction-based CASSCF/CASPT2 calculations[39–43] were performed including spin-orbit coupling, together with effective core potentials for all atoms.[44,45] All these calculations have been carried out using the MOLCAS 8.0 suite of programs.[46] The structural parameters of the calculated clusters are collected in Table I.

Vertical detachment energies (VDEs) were calculated to compare with the experimental data. The first VDE for each species was calculated as the energy difference between the anion and neutral states at the corresponding anion equilibrium geometry.[47] The simulated spectra presented in Figs. 1 and 2 were obtained by fitting each of the computed VDEs with a Gaussian function of 0.04 eV width.

III. RESULTS

A. Photoelectron spectra at 193 nm

Figs. 1(a) and 2(a) show the PE spectra of AuC_4^- and AuC_6^-, respectively, at 193 nm using the magnetic-bottle apparatus. The two spectra are similar with numerous intense detachment bands, which are labeled with letters X and A—H. The VDEs of the X bands in both species are quite high, at ∼3.5 eV for AuC_4^- and ∼3.6 eV for AuC_6^-, and the X and A bands are not resolved in the 193 nm spectra. At higher binding energies, more bands are observed. The adiabatic detachment energies (ADEs) and VDEs of the observed bands are given in Table II, where the more accurate data are from high-resolution PE imaging to be presented below.

For the spectra of both AuC_4^- and AuC_6^-, a very weak band (feature X′) is observed in the lower binding energy

TABLE II. Experimental adiabatic (ADE) and vertical (VDE) detachment energies from the ground state of AuC_n^- and AuC_nH^- to that of their neutrals, their assignments, and comparison with the calculated values using the B3LYP density functional. Values marked by * are from adding the SO term calculated at CASSCF/CASPT2 to the ADEs.

			ADE (eV)		VDE (eV)	
	Observed feature	Final state	Expt.[a]	Theo.	Expt.[a]	Theo.
AuC_4^-	X	$^2\Pi_{3/2}$	3.366	3.20	3.494	3.30
	A	$^2\Pi_{1/2}$	3.413	3.41*	…	…
AuC_6^-	X	$^2\Pi_{3/2}$	3.593	3.40	3.611	3.51
	A	$^2\Pi_{1/2}$	3.636	3.58*	…	…
AuC_2H^-	X′	^1A	1.475	1.47	1.500	1.59
AuC_4H^-	X′	^1A	1.778	1.79	1.990	1.91
AuC_6H^-	X′	^1A	1.962	2.02	2.060	2.13

[a] Experimental uncertainties were estimated to be ±0.001 eV.

region at ∼2.0 eV. The relative intensities of these features are no more than ∼5%-10% of the main spectral bands. Similar weak features were also observed in our previous study of AuC_2^- at 193 nm and they were interpreted as due to excited states of AuC_2^-,[22] following a prior study by Visser *et al.*[48] However, a subsequent study by S. G. He (private communication) suggested that the weak features in AuC_2^- were in fact due to the AuC_2H^- impurity. Hence, the similar weak features in the AuC_4^- and AuC_6^- spectra may also come from hydride impurities; their high-resolution PE imaging data will be presented below. Figs. 1(b), 1(c), 2(b), and 2(c) show the simulated PE spectra for the AuC_4^-, AuC_4H^-, AuC_6^-, and AuC_6H^- ground states, respectively. Overall, good agreement is seen between the simulated spectra and the experimental data. The peaks X, A, B, and G in Fig. 1(a) match well with those of AuC_4^- while the computed transitions from AuC_4H^- are consistent with the weak features, in particular the weak X′ feature. Similarly, the peaks X, A, C, G, and H in Fig. 2(a) match well with those of AuC_6^-, while features X′, B, D, E, and F seem to be due to AuC_6H^-.

B. High resolution photoelectron imaging of bands X and A

The PE images and spectra of AuC_4^- and AuC_6^- at 3.6905 eV are shown in Figs. 3(a) and 4(a), respectively, covering the spectral region of the two strong bands X and A revealed in the 193 nm spectra. The spectrum of AuC_4^- is highly congested with numerous vibrational fine features (labeled as *a* to *f*), suggesting significant geometry changes between the ground state of AuC_4^- and that of its neutral. Additionally, peaks *d*, *e*, and *f* seem to consist of a doublet, as can be seen under even higher resolution at low photon energies (Figs. 3(b) and 3(c)). The high-resolution spectrum of AuC_6^- is less congested, and only five features (labeled as *a* to *e*) are observed at 3.6905 eV (Fig. 4(a)). The peaks in the spectra of both AuC_4^- and AuC_6^- are separated by different spacings and are probably due to different bending modes of two different electronic states. Even under the high-resolution condition at 3.4501 eV (Fig. 3(c)), the spectrum of AuC_4^- still displays a complex pattern. The absence of any vibrational hot bands suggests that our cluster beam was quite cold vibrationally.

The angular distributions of the PE images for AuC_4^- (Fig. 3) and AuC_6^- (Fig. 4) are isotropic with a β parameter oscillating around a value of zero for different kinetic energies. The binding energies for all the observed peaks in Figs. 3 and 4 are summarized in Table III. Accurate ADEs and VDEs from the high-resolution imaging data for bands X and A are given in Table II, in comparison with the theoretical data.

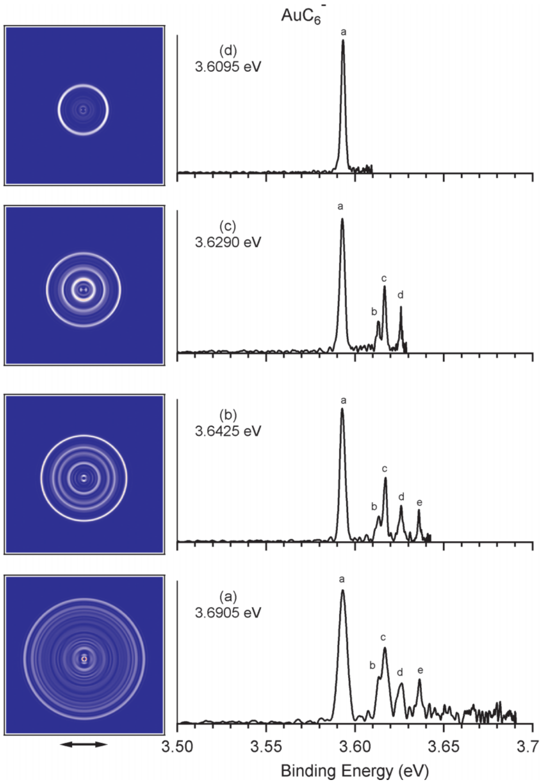

FIG. 4. High-resolution PE images and spectra of AuC_6^- at photon energies of (a) 3.6905 eV, (b) 3.6425 eV, (c) 3.6290 eV, and (d) 3.6095 eV. The left panels show the PE images after inverse-Abel transformation. The double arrows indicate the polarizations of the laser.

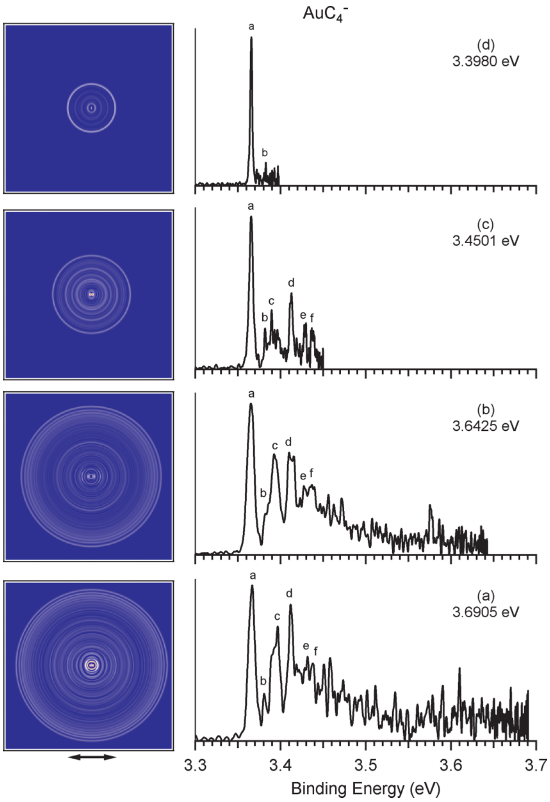

FIG. 3. High-resolution PE images and spectra of AuC_4^- at photon energies of (a) 3.6905 eV, (b) 3.6425 eV, (c) 3.4501 eV, and (d) 3.3980 eV. The left panels show the PE images after inverse-Abel transformation. The double arrows indicate the polarizations of the laser.

C. High-resolution imaging of bands X′ for AuC_4H^- and AuC_6H^-

The comparison between the simulated spectra and the experimental data in Figs. 1 and 2 indicates that the weak X′ band in the AuC_4^- and AuC_6^- spectra was due to the AuC_4H^- and AuC_6H^- contamination, respectively. Figs. 5

TABLE III. Observed binding energies from the high-resolution photoelectron spectra of AuC_4^- (Fig. 3) and AuC_6^- (Fig. 4).

		AuC_4^-		
	Binding energies[a]			
Observed peaks	eV	cm^{-1}	Separation from the first peak (cm^{-1})	Assignment ($\nu_1\ \nu_2\ \nu_3$)
a	3.366	27 147	...	$^2\Pi_{3/2}$ (000)
b	3.382	27 276	129	$^2\Pi_{3/2}$ (010)
c	3.390	27 339	192	$^2\Pi_{3/2}$ (001)
d	3.413	27 525	378	$^2\Pi_{3/2}$ (100) + $^2\Pi_{1/2}$ (000)
e	3.429	27 655	508	$^2\Pi_{1/2}$ (010)
f	3.438	27 725	578	$^2\Pi_{1/2}$ (001)
		AuC_6^-		
	Binding energies[a]			
Observed peaks	eV	cm^{-1}	Separation from the first peak (cm^{-1})	Assignment ($\nu_1\ \nu_2\ \nu_3\ \nu_4$)
a	3.593	28 982	...	$^2\Pi_{3/2}$ (0000)
b	3.613	29 141	159	$^2\Pi_{3/2}$ (0010)
c	3.617	29 170	188	$^2\Pi_{3/2}$ (0001)
d	3.626	29 245	263	$^2\Pi_{3/2}$ (1000)
e	3.636	29 326	344	$^2\Pi_{1/2}$ (0000)

[a] The peak positions have an uncertainty of ±0.001 eV.

and 6 show the high-resolution PE images and spectra of the weak X′ bands, corresponding to the ground state detachment transition of AuC_4H^- and AuC_6H^-, respectively. Figs. 5(a) and 6(a) show that each spectrum consists of a long vibrational progression with seven well-resolved peaks for AuC_4H^- (labeled as a'–g') and six in the case of AuC_6H^- (labeled as a'_1–f'_1). The average spacing of the peaks in the AuC_4H^- spectra is about 340 cm^{-1}. Interestingly, fine features are further resolved for AuC_6H under high resolution, when the detachment laser is tuned close to each of the vibrational peaks in band X' (Fig. 6). Each of the main features is accompanied by another weak feature (labeled as a'_2–f'_2). The separation between the main features is about 260 cm^{-1}, while the separation between each of the weak features and that of the main features is about 60 cm^{-1}.

All the β values show an isotropic distribution for the low kinetic energy peaks, while the angular distributions lie slightly parallel to the laser polarization ($\beta > 0$) at higher kinetic energies.

D. Theoretical results

We carried out both DFT and wavefunction-based CASSCF/CASPT2 calculations including spin-orbit coupling to facilitate the interpretation of our new PES data, particularly for the origins of the weak X′ band observed in the 193 nm spectrum for AuC_4^- (Fig. 1(a)) and AuC_6^- (Fig. 2(a)). We have optimized different types of structures for AuC_4, AuC_4^-, AuC_6, and AuC_6^- and found only the linear/bent Au—C_n arrangements to be relevant. We find that the global minima of both AuC_4^- and AuC_6^- are bent ($^1A'$), while their neutral ground states are linear ($^2\Pi$). Similarly, both AuC_4H^- and AuC_6H^- are found to be linear in the anion ($^2\Sigma$) and neutral ground states ($^1\Sigma$). The energetics of the two AuC_4 and AuC_6

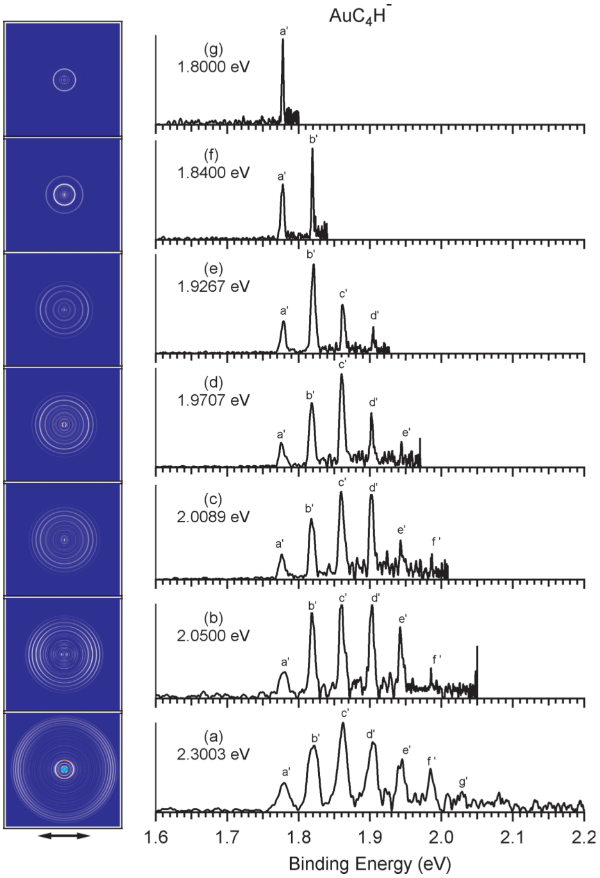

FIG. 5. High-resolution PE images and spectra of AuC_4H^- at photon energies of (a) 2.3003 eV, (b) 2.0500 eV, (c) 2.0089 eV, (d) 1.9707 eV, (e) 1.9267, (f) 1.8400, and (g) 1.8000 eV. The left panels show the PE images after inverse-Abel transformation. The double arrows indicate the polarizations of the laser.

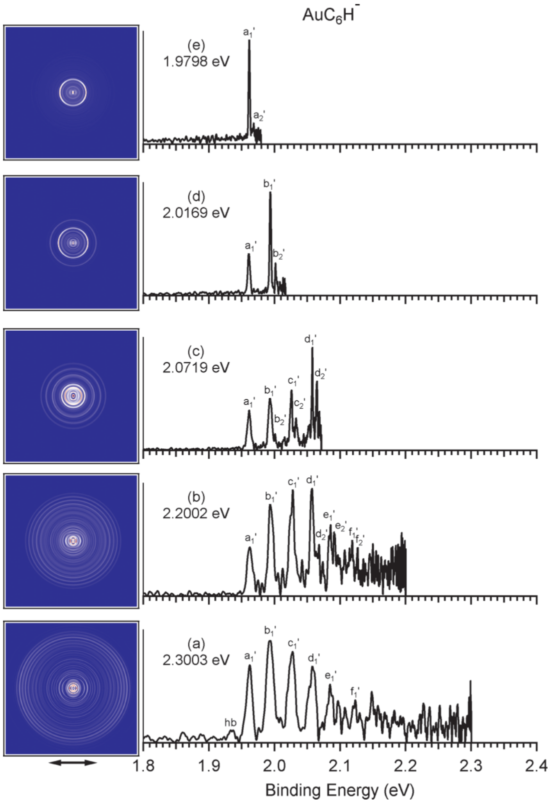

FIG. 6. High-resolution PE images and spectra of AuC_6H^- at photon energies of (a) 2.3003 eV, (b) 2.2002 eV, (c) 2.0719 eV, (d) 2.0169 eV, and (e) 1.9798 eV. The left panels show the PE images after inverse-Abel transformation. The double arrows indicate the polarizations of the laser.

neutral states relative to their respective anion global minima are calculated to be 3.13 and 3.04 eV. DFT calculations show a slightly different value and the respective ADE was calculated to be 3.2 and 3.4 eV, respectively. The SO splitting between the $^2\Pi_{3/2}$ and $^2\Pi_{1/2}$ states for AuC_4 and AuC_6 is calculated to be 21 and 18 meV, respectively. The energetics of the AuC_2H, AuC_4H, and AuC_6H neutral states with respect to their anion global minima are calculated to be 1.47, 1.79, and 2.02 eV, respectively. The relative energies, geometrical parameters, and vibrational frequencies of the computed states for all the structures are collected in Table I, whereas Figure 7 shows all the anion and neutral structures along with the relevant bond lengths.

We carried out Franck-Condon (FC) simulations for the different PE spectra, which are shown in Figs. S1–S5 in the supplementary material.[49] The simulations were done using the PESCAL program,[50] which computes FC factors by numerical integration of vibrational wavefunctions of a properly fitted Morse oscillator.

IV. DISCUSSION

A. High resolution PE imaging of AuC_4^-

Fig. 8 shows the valence molecular orbitals of AuC_n^- and AuC_nH^-. The X band is due to electron detachment from the 10π HOMO, leading to the $^2\Pi$ ground state for neutral AuC_4. The high-resolution data presented in Fig. 3 display complicated vibrational structures for the ground state

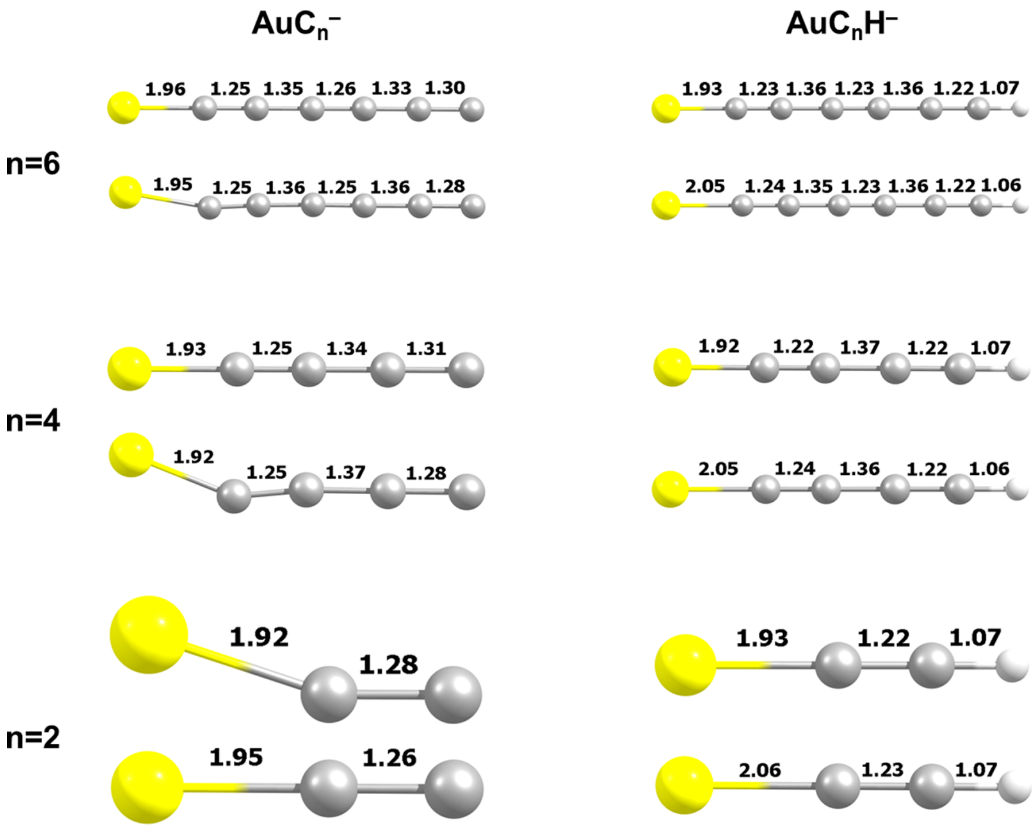

FIG. 7. Structures and bond lengths of AuC_n^- and AuC_nH^- ($n = 2$, 4, and 6) and their corresponding neutrals. For each species, the bottom shows the anion structure, while the top structure is for the neutral. All bond distances are given in Å.

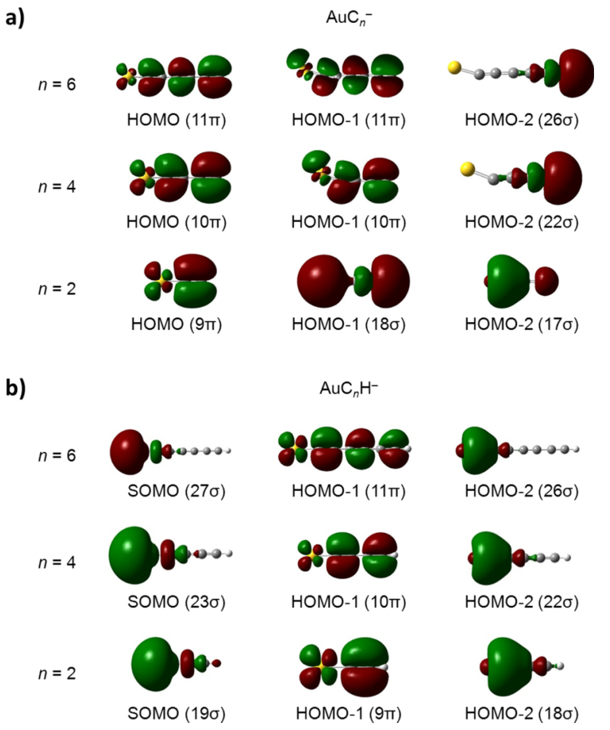

FIG. 8. The top three valence molecular orbitals of (a) AuC$_n^-$ ($n = 2$, 4, and 6) and (b) AuC$_n$H$^-$ ($n = 2$, 4, and 6).

detachment transition due to excitations of several vibrational modes. Additionally, the two spin-orbit components of the $^2\Pi$ final state are calculated to be separated by only 21 meV, which is on the order of the vibrational frequencies and complicates the assignment. Table III shows that indeed the ground state consists of features spaced in different amounts. The spacing between the peaks *a* and *b* is 129 cm^{-1}, peaks *a-c* are separated by 192 cm^{-1} and the separation between peaks *a* and *d* is 378 cm^{-1}. The 129 cm^{-1} value is very close to the lowest bending mode calculated at 102 cm^{-1}; the 192 cm^{-1} spacing could be due to the asymmetric bending mode calculated at 248 cm^{-1}. Finally, the 378 cm^{-1} value is quite close to the Au—C stretching mode calculated at 339 cm^{-1}.

To help interpret the complicated spectra of AuC$_4^-$, we carried out FC simulations (Fig. S1).[49] Figs. S1(a) and S1b[49] show a reasonable comparison between a FC simulation using three active vibrational modes and the experimental spectra at two different photon energies. However, the simulation cannot explain the appearance of the SO-splitted term, as revealed by the double peaks, such as peaks *d*, *e*, and *f*. Figs. S1(c) and S1d[49] show a simulated spectrum with only two bending modes and with the *d* feature as the origin of the $^2\Pi_{1/2}$ state. However, this simulation still cannot explain the doublet structure of some peaks. Finally, Figs. S1(e) and S1f[49] show a FC simulation as that in Fig. S1(a),[49] but including the SO-splitted term shifted by a few wavenumbers from peak *d*. The comparison shows a remarkably good fit both in shape and in that it also explains the observed doublet peaks. The simulations suggest that the observed spectra for AuC$_4^-$ consist of a combination of a stretching and two bending modes and two different SO-splitted states with similar vibrational progressions. It also explains the congested vibrational structures seen at higher binding energies (>3.45 eV). Therefore, we assign peak *a* as the origin of the $^2\Pi_{3/2}$ state and peak *d* as the origin of the $^2\Pi_{1/2}$ state, giving rise to an experimental SO coupling constant of 378 cm^{-1}. The measured ADE from peak *a* is 3.366 ± 0.001 eV (Table II).

Both the threshold behavior which indicates that the intensity does not drastically reduce near the threshold and the β parameters for the vibrational features are consistent with detachment from the 10π orbital, which would produce outgoing electrons with $l = 0$ (*s*-wave) or 2 (*d*-wave).

B. High resolution PE imaging of AuC$_6^-$

Similar to AuC$_4^-$, the X band of AuC$_6^-$ corresponds to electron detachment from the 11π HOMO (Fig. 8), resulting in a $^2\Pi$ state for neutral AuC$_6$. The high-resolution spectra shown in Fig. 4 are much less congested in comparison to those of AuC$_4^-$. The separation between the two spin-orbit components of the $^2\Pi$ final state is calculated to be only 19 meV. Table III lists all the binding energies of all the observed peaks and their assignments. Peak *a* corresponds to the origin of the $^2\Pi_{3/2}$ state, defining an accurate EA of 3.593 ± 0.001 eV for AuC$_6$. Peaks *a* and *b* are separated by 159 cm^{-1}; peaks *a-c* are separated by 188 cm^{-1}. These values are very close to the calculated bending modes of 134 and 156 cm^{-1}, respectively (Table I). The spacing between peaks *a-d* is 263 cm^{-1}, which is close to both the 277 cm^{-1} bending mode and the Au—C stretching mode calculated at 269 cm^{-1}. Based on the similarity of the HOMO of AuC$_6^-$ and AuC$_4^-$, the Au—C stretching mode should also be active in the ground state detachment transition. Hence, it is more reasonable to assign the 263 cm^{-1} mode to the Au—C stretch. However, peak *e*, separated from feature *a* by 344 cm^{-1}, does not correspond to any of the calculated vibrational frequencies.

The simulated FC spectrum (Fig. S2[49]) indicates that a progression based on three modes (two bending modes + the stretching mode) shows a doublet instead of a single peak near peak *e*. A more likely explanation is that peak *e* corresponds to the origin of the $^2\Pi_{1/2}$ state. The SO coupling constant of 344 cm^{-1} is similar to the 378 cm^{-1} value obtained for AuC$_4$, consistent with the calculations that also show a similar SO splitting for both AuC$_4^-$ and AuC$_6^-$ with a slightly lower value for AuC$_6$ (*vide infra*). The absence of vibrational progressions for the $^2\Pi_{1/2}$ state is likely due to its weak intensity. In fact, Fig. 4(a) shows discernable electron signals beyond 3.65 eV, but the low signal-to-noise ratios do not allow any definitive assignment.

Similar to that for AuC$_4^-$, the threshold behavior and the β parameters are also consistent with detachment from the 11π orbital, producing outgoing electrons with $l = 0$ (*s*-wave) or 2 (*d*-wave).

C. High-resolution PE imaging of AuC$_4$H$^-$

The X′ band observed in Fig. 1(a) is assigned to electron detachment from the 23σ singly occupied molecular orbital (SOMO) of AuC$_4$H$^-$ (Fig. 8), which involves an antibonding σ orbital between Au and carbon. The high-resolution data presented in Fig. 5 show a vibrational progression with a

TABLE IV. Observed binding energies from the high-resolution photoelectron spectra of AuC_4H^- (Fig. 5) and AuC_6H^- (Fig. 6).

AuC_4H^-

Observed peaks	Binding energies[a] eV	Binding energies[a] cm^{-1}	Separation from consecutive peaks (cm^{-1})	Assignment (ν_1 ν_2 ν_3)
a′	1.778	14 340	…	000
b′	1.819	14 674	334	100
c′	1.861	15 013	339	200
d′	1.904	15 361	348	300
e′	1.944	15 678	317	400
f′	1.987	16 023	345	500
g′	2.029	16 365	342	600

AuC_6H^-

Observed peaks	Binding energies[a] eV	Binding energies[a] cm^{-1}	Peaks separation of the main and minor progressions (cm^{-1})	Assignment (ν_1 ν_2 ν_3)
a'_1	1.962	15 822	…	000
a'_2	1.968	15 877	55	010
b'_1	1.994	16 081	259	100
b'_2	2.002	16 144	63	110
c'_1	2.026	16 341	260	200
c'_2	2.033	16 397	56	210
d'_1	2.058	16 597	256	300
d'_2	2.065	16 654	57	310
e'_1	2.085	16 820	223	400
e'_2	2.091	16 868	48	410
f'_1	(2.119)	17 088	268	500
f'_2	(2.127)	17 155	67	510

[a] The peak positions have an uncertainty of ±0.001 eV.

broad FC profile. The *a′* peak should correspond to the 0-0 transition, defining an accurate EA of 1.778 ± 0.001 eV for AuC_4H. Table IV lists the binding energies of all the observed peaks, which have a constant spacing of approximately 340 cm^{-1}. Both the anion and neutral are linear and hence only stretching modes should be active. The calculated Au—C stretching frequency of neutral AuC_4H is 338 cm^{-1}, in excellent agreement with the observed vibrational spacing. The simulated FC spectrum in Fig. S3[49] agrees well with the experimental data. The long Au—C stretching progression is consistent with the large Au—C bond length change between the anion and neutral ground states (Table I and Figure 7).

As shown in Fig. 5, the anisotropy parameter is close to zero at low kinetic energies, while it increases at high kinetic energies although β remains lower than 1 ($0 < \beta < 1$). The observed *p*-wave character at high kinetic energies is consistent with the σ SOMO of AuC_4H^- (Fig. 8).

D. High-resolution PE imaging of AuC_6H^-

Fig. 6 shows the PE images and spectra of AuC_6H^- at five photon energies, also revealing a long vibrational progression, similar to that for AuC_4H^-. The detachment should be from the 27σ SOMO of AuC_6H^-, which is mainly an antibonding σ orbital between gold and carbon (Fig. 8). The high-resolution spectra reveal that there is a weaker feature close to each main peak. Table IV lists the binding energies of all the observed features. The a'_1 peak should correspond to the 0-0 transition, yielding an accurate EA of 1.962 ± 0.001 eV for AuC_6H. The main vibrational progression has a constant spacing of approximately 260 cm^{-1}, while the weak feature is separated from the main peak by approximately 55 cm^{-1}. As in the case of AuC_4H^-, both the AuC_6H^- anion and its neutral are linear and hence only stretching modes should be active. The calculated Au—C stretching frequency of the neutral is 266 cm^{-1} in excellent agreement with the main vibrational progression. The minor feature agrees with the lowest bending mode of 55 cm^{-1}, suggesting that either neutral AuC_6 or its anion might be slightly bent. An FC simulation using the Au—C stretching and bending modes agrees well with the observed spectra, as shown in Fig. S4.[49]

The SOMO of AuC_6H^- is a σ orbital, which results in an outgoing electron with $l = 1$. The observed *p*-wave character at high kinetic energies is consistent with the σ SOMO of AuC_6H^- (Fig. 8).

E. Comparison of $AuC_n{}^-$ with $HC_n{}^-$

It is interesting to compare the results of $AuC_n{}^-$ with those of HC_n^-. The ground state of C_2H is $^2\Sigma^+$, and the $^2\Pi$ excited state is at 3700 cm^{-1}.[51–54] On the other hand, the spectroscopy of C_4H showed that the $^2\Sigma^+$ and $^2\Pi$ states are nearly degenerate, only separated by 213 cm^{-1}, and there is evidence of vibronic interaction between the two states.[55] In

C_6H, the order is reversed and the $^2\Pi$ state is the ground state of the neutral, while the $^2\Sigma^+$ state lies 1500 cm^{-1} above.[56,57] It is interesting to observe that the switch of the relative energetic order between these states happens less with Au atoms than in the species with hydrogen. For AuC_2 we already observed that the separation between the neutral ground state and the excited state was only about 17 cm^{-1}.[22] Additionally, there were indications of strong vibronic coupling. While the ground state of AuC_2^- is linear ($^1\Sigma^+$), the corresponding ground state, $^2\Sigma^+$, of the neutral species was shown to be bent, as a result of strong vibronic interactions with the nearby $^2\Pi$ excited state via strong spin-orbit coupling. In the current work we show that for the AuC_4 cluster the energetic order of the states is already reversed and the neutral ground state is a $^2\Pi$ state.

Another important observation is the fact that when hydrogen is replaced by gold the neutral structure remains similar (although for AuC_2 the neutral was found to be bent due to the strong vibronic interactions) but for $AuC_{4,6}$ their anions are bent.

A further confirmation about the Au/H analogy lies in the EA trend as the length of the carbon chain is increased. For HC_n, the EAs are 2.969, 3.533, and 3.809 eV for HC_2, HC_4, and HC_6, respectively.[54–56] The EA values are 3.219, 3.366, and 3.593 eV for AuC_2,[22] AuC_4, and AuC_6, respectively (Table II). There is an approximate increase of about 100 meV per carbon atom added. The current results further reinforce the Au/H analogy in the Au—C bonding.

F. AuC_nH^- (n = 2, 4, and 6)

In one of our previous works[22] as well as in Ref. 48, the weak feature appearing around 1.5 eV was assigned erroneously to a metastable excited state of AuC_2^-. It is not surprising that the binding energy of the first excited state in AuC_2^- is similar to that of the AuC_2H^- anion ground state, which, in fact, further confirms the Au/H analogy. The weak X′ band around 1.5 eV was due to vibrational progressions of the $AuC_2H \leftarrow AuC_2H^-$ transition based on a combination of the stretching and the even bending modes of the neutral (separations of 445 cm^{-1} and 520 cm^{-1}, respectively), which match reasonably well with the calculated values (485 and 259 × 2 cm^{-1}, respectively) (Table I). In fact, the close proximity of the stretching and even quanta of the bending mode leads to Fermi resonances and hence the unusual high intensity of the bending progression. Figure S5[49] presents a comparison between the calculated Franck-Condon factors and the experimental spectrum at 1.6850 eV that shows very good agreement between the experiment and the simulation.

The EA values are 1.475, 1.778, and 1.962 eV for AuC_2H, AuC_4H, and AuC_6H, respectively. Interestingly, similar to the AuC_n series there is also an approximate increase of about 150 meV per carbon atom added.

The comparison with the HC_nH species is interesting as the latter do not bind an electron. The introduction of Au makes a big difference in terms of the electronic structure: the SOMO of AuC_nH^- shows that the main contribution comes from the Au 6s orbital (Fig. 8). It is understandable that it is easier to add an electron to the Au-containing species than in HC_nH, whose LUMO is at much higher energies. Hence, the contribution of Au to the LUMO in AuC_nH adds much stabilization to allow strong electron binding.

G. Comparison of the chemical bonding in $Au—C_n^-$ and $Au—C_nH^-$ with that in $ClAu—CCH^-$

The bond dissociation energies of AuC_n^- in $AuC_n^- \rightarrow Au + C_n^-$ for n = 2, 4, and 6 are calculated to be 2.80, 2.13, and 1.97 eV, respectively. There is a decrease in the bond strength as the number of carbon atoms is increased; particularly, there is a remarkable difference between two and four carbons. The 2.80 eV dissociation energy of AuC_2^- shows that it is much smaller than the 4.52 eV or 5.23 eV dissociation energies for $ClAu—CCH^-$ ($^1\Sigma^+$) → $ClAu$ ($^1\Sigma^+$) + CCH^- ($^1\Sigma^+$) or $ClAu—CCH^-$ ($^1\Sigma^+$) → $ClAu^-$ ($^2\Sigma^+$) + CCH ($^2\Sigma^+$), highlighting once more the importance of the auxiliary ligand (L) in influencing the Au—C bond in $LAu—CCH^-$. Finally, the dissociation energies of AuC_nH^- in $AuC_nH^- \rightarrow Au + C_nH^-$ for n = 2, 4, and 6 are 1.95, 1.67, and 1.46 eV, respectively. These values reveal a decrease by ∼33% in the strength of the Au—C bond in AuC_nH^- than in AuC_n^-. There is a slight decrease of the binding energy as the number of carbons is increased in AuC_nH^-, about 0.2 eV per C_2 added. The most meaningful information is obtained by comparing the dissociation energy of $LAu—CCH^-$ and that of $Au—CCH^-$ as it gives a straightforward estimation of the influence of the auxiliary ligand on the Au—C bonding strength. The 4.52 eV value of the former is more than twice the 1.95 eV value of $Au—CCH^-$, highlighting the importance of polarization of the Au center by the auxiliary ligand L, resulting in an unusually strong Au—C bond in $LAu—CCH^-$.[15]

The SOMO of AuC_nH^- involves Au—C antibonding interactions (Fig. 8), leading to weaker Au—C bonding in the anion. Hence, we also calculated the Au—C bond energy in neutral $Au—C_nH$. The Au—C bond dissociation energies of $AuC_nH \rightarrow Au + C_nH$ for n = 2, 4, and 6 are 3.84, 3.30, and 3.06 eV, respectively, significantly stronger than that in the anion. The dependence on the carbon chain length is the same as in the anion: there is a decrease in the dissociation energy as n increases.

H. Energy decomposition analysis (EDA)

In order to further analyze the nature of the chemical bonding in the AuC_n^- molecules, we have performed an energy decomposition analysis (EDA).[58,59] The interaction energy (ΔE_{int}) of two fragments A and B in the molecule A-B is decomposed into three contributions: the Pauli repulsion (ΔE_{Pauli}), the electrostatic interaction (ΔE_{elstat}), and the orbital attraction (ΔE_{orb}), which can be identified as the covalency contribution to the chemical bond. Table V shows the results of the analysis.

The EDA shows that both covalent (50.1%) and ionic (49.9%) interactions in the Au—C chemical bond in AuC_2^- are on an equal footing. However, for AuC_4^- and AuC_6^-, the covalent contribution decreases, resulting in the weaker Au—C bond in the longer chain complexes.

TABLE V. Energy decomposition analyses of the Au—C bond. All values in kcal/mol. Values in parentheses give the percentage contribution to the total attractive interactions $\Delta E_{elstat} + \Delta E_{orb}$.

	AuC_2^-	AuC_4^-	AuC_6^-
ΔE_{int}	−92.60	−78.25	−72.11
ΔE_{Pauli}	311.79	337.76	339.67
ΔE_{elstat}	−200.97 (49.9%)	−237.70 (57.4%)	−236.29 (57.6%)
ΔE_{orb}	−202.10 (50.1%)	−176.74 (42.6%)	−173.84 (42.4%)

V. CONCLUSIONS

We report high-resolution photoelectron spectroscopy and imaging of AuC_n^- (n = 4 and 6) and AuC_nH^- (n = 2, 4, and 6) in a wide photon energy range. The 193 nm spectrum of the AuC_n^- clusters revealed several major detachment bands, as well as very weak low electron binding energy features due to the AuC_nH^- species, which were present as minor impurities. The ground states of the AuC_n^- systems are bent, while the neutral ground states are found to be linear. On the other hand, the AuC_nH^- species have a linear configuration in both the anion and neutral states. The electron affinities are measured accurately to be 3.366(1) and 3.593(1) eV for AuC_4 and AuC_6, respectively, while the values are 1.475(1), 1.778(1), and 1.962(1) eV for AuC_nH, n = 2, 4, and 6, respectively. In AuC_4 the active bending frequencies are found to be 129(10) and 192(10) cm^{-1} with a stretching frequency of 378(11) cm^{-1}. In AuC_6 the bending modes are 159(11) and 188(11) cm^{-1} with a rather low Au—C stretching frequency of 263(11) cm^{-1}. The high-resolution PE spectra of the AuC_nH^- species show a vibrational progression in the Au—C stretching mode: the spectra of AuC_2H^- show a progression in the stretching mode of 445(10) cm^{-1} along with Fermi resonances of the bending frequency of 260 cm^{-1}. The high-resolution PE spectra of AuC_4H^- reveal a ground state Au—C stretching frequency of 340(10) cm^{-1} in AuC_4H. The spectra of AuC_6H^- show a ground state Au—C stretching frequency of 260(10) cm^{-1} together with a bending frequency of 55(10) cm^{-1} for AuC_6H. The AuC_2^- complex features the strongest Au—C bond among the three species, and the Au—C bond strength is found to decrease as the number of carbon atoms is increased. The EDA shows that the covalent contribution to the chemical bond in AuC_2^- is higher than for AuC_4^- and AuC_6^-, consistent with the weaker Au—C bonds in the latter.

ACKNOWLEDGMENTS

We thank Dr. Z. Yang for experimental assistance. I.L. would like to thank the MINECO for a Juan de la Cierva postdoctoral fellowship. We thank Professor Sheng-Gui He for sharing his initial data on AuC_2H^-. This work was supported by the National Science Foundation (to L.S.W.). We are also grateful to IZO-SGI, SGIker (UPV/EHU, MICINN, GV/EJ, ERDF, and ESF) for both technical and personal support and for generous allocation of computational resources.

[1] P. Pyykko, Chem. Rev. **88**, 563 (1988).
[2] H. Schmidbaur, Gold Bull. **33**, 3 (2000).
[3] G. J. Hutching, M. Brust, and H. Schmidbaur, Chem. Soc. Rev. **37**, 1759 (2008).
[4] L. S. Wang, Phys. Chem. Chem. Phys. **12**, 8694 (2010).
[5] B. Kiran, X. Li, H. J. Zhai, and L. S. Wang, J. Chem. Phys. **125**, 133204-1–133204-7 (2006).
[6] R. Pal, L. M. Wang, W. Huang, L. S. Wang, and X. C. Zeng, J. Am. Chem. Soc. **131**, 3396–3404 (2009).
[7] L. M. Wang, S. Bulusu, W. Huang, R. Pal, L. S. Wang, and X. C. Zeng, J. Am. Chem. Soc. **129**, 15136–15137 (2007).
[8] D. Y. Zubarev, A. I. Boldyrev, J. Li, H. J. Zhai, and L. S. Wang, J. Phys. Chem. A **111**, 1648–1658 (2007).
[9] D. Y. Zubarev, J. Li, L. S. Wang, and A. I. Boldyrev, Inorg. Chem. **45**, 5269–5271 (2006).
[10] A. S. K. Hashmi, Chem. Rev. **107**, 3180 (2007).
[11] G. J. Gorin, B. D. Sherry, and F. D. Toste, Chem. Rev. **108**, 3351 (2008).
[12] E. Jimenez-Nunez and A. M. Echavarren, Chem. Rev. **108**, 3326 (2008).
[13] Z. G. Li, C. Brouwer, and C. He, Chem. Rev. **108**, 3239 (2008).
[14] A. Corma, A. Leyva-Perez, and M. J. Sabater, Chem. Rev. **111**, 1657 (2011).
[15] H. T. Liu, X. G. Xiong, P. D. Dau, Y. L. Wang, D. L. Huang, J. Li, and L. S. Wang, Nat. Commun. **4**, 2223 (2013).
[16] K. K. Irikura and W. A. Goddard, J. Am. Chem. Soc. **116**, 8733 (1994).
[17] H. Schwarz, Angew. Chem., Int. Ed. **42**, 4442 (2003).
[18] P. Pyykkö and T. Tamm, Theor. Chem. Acc. **99**, 113 (1998).
[19] M. Barysz and P. Pyykkö, Chem. Phys. Lett. **285**, 398 (1998).
[20] C. Puzzarini and K. A. Peterson, Chem. Phys. **311**, 177 (2005).
[21] H. G. Cho and L. Andrews, Inorg. Chem. **50**, 10319 (2011).
[22] I. León, Z. Yang, and L. S. Wang, J. Chem. Phys. **140**, 084303 (2014), note: The assignment of the weak low-binding energy features to excited states of AuC_2^- was incorrect in this reference. They were in fact due to AuC_2H^- presented in the cluster beam as an impurity, see Section III A in the text.
[23] I. León, Z. Yang, H. T. Liu, and L. S. Wang, Rev. Sci. Instrum. **85**, 083106 (2014).
[24] L. S. Wang, H. S. Cheng, and J. W. Fan, J. Chem. Phys. **102**, 9480 (1995).
[25] I. León, Z. Yang, and L. S. Wang, J. Chem. Phys. **138**, 184304 (2013); Erratum, **139**, 089903 (2013).
[26] Z. Yang, I. León, and L. S. Wang, J. Chem. Phys. **139**, 021106 (2013).
[27] I. León, Z. Yang, and L. S. Wang, J. Chem. Phys. **139**, 194306 (2013).
[28] W. Huang and L. S. Wang, Phys. Rev. Lett. **102**, 153401 (2009).
[29] H. J. Zhai, B. Kiran, and L. S. Wang, J. Chem. Phys. **121**, 8231 (2004).
[30] V. Dribinski, A. Ossadtchi, V. A. Mandelshtam, and H. Reisler, Rev. Sci. Instrum. **73**, 2634 (2002).
[31] G. A. Garcia, L. Nahon, and I. Powis, Rev. Sci. Instrum. **75**, 4989 (2004).
[32] M. J. Frisch *et al.*, GAUSSIAN 09, Revision A.2, Gaussian, Inc., Wallingford, CT, 2009.
[33] A. D. Becke, J. Chem. Phys. **98**, 5648 (1993).
[34] C. Lee, W. Yang, and R. G. Parr, Phys. Rev. B **37**, 785 (1988).
[35] W. J. Hehre, R. Ditchfield, and J. A. Pople, J. Chem. Phys. **56**, 2257 (1972).
[36] P. J. Hay and W. R. Wadt, J. Chem. Phys. **82**, 270 (1985).
[37] W. R. Wadt and P. J. Hay, J. Chem. Phys. **82**, 284 (1985).
[38] P. J. Hay and W. R. Wadt, J. Chem. Phys. **82**, 299 (1985).
[39] B. O. Roos, P. R. Taylor, and P. E. M. Siegbahn, Chem. Phys. **48**, 157 (1980).
[40] P. E. M. Siegbahn, A. Heiberg, J. Almlöf, and B. O. Roos, J. Chem. Phys. **74**, 2384 (1981).
[41] P. E. M. Siegbahn, A. Heiberg, B. O. Roos, and B. Levy, Phys. Scr. **21**, 323 (1980).
[42] K. Andersson, P.-Å. Malmqvist, B. O. Roos, A. J. Sadlej, and K. Wolinksi, J. Phys. Chem. **94**, 5483 (1990).
[43] K. Andersson, P.-Å. Malmqvist, and B. O. Roos, J. Chem. Phys. **96**, 1218 (1992).
[44] Z. Barandiarán and L. Seijo, Can. J. Chem. **70**, 409 (1992).
[45] M. Casarrubios and L. Seijo, J. Chem. Phys. **110**, 784 (1999).
[46] F. Aquilante, L. De Vico, N. Ferré, G. Ghigo, P.-Å. Malmqvist, P. Neogrády, T. B. Pedersen, M. Pitoňák, M. Reiher, B. O. Roos, L. Serrano-Andrés, M. Urban, V. Veryazov, and R. Lindh, J. Comput. Chem. **31**, 224 (2010).
[47] X. Li, B. Kiran, J. Li, H. J. Zhai, and L. S. Wang, Angew. Chem., Int. Ed. **41**, 4786 (2002).
[48] B. R. Visser, M. A. Addicoat, J. R. Gascooke, W. D. Lawrance, and G. F. Metha, J. Chem. Phys. **138**, 174310 (2013), note: In light of the current study, the observed species in this reference should be due to AuC_2H^-, rather than an excited state of AuC_2^-, see the note in Ref. 22 and Section III A in the text.

[49] See supplementary material at http://dx.doi.org/10.1063/1.4960440 for a comparison of the Franck-Condon (FC) simulations for the different PE spectra.

[50] K. M. Ervin, Fortran program, PESCAL, 2010.

[51] R. F. Curl, P. G. Carrick, and A. J. Merer, J. Chem. Phys. **82**, 3479 (1985).

[52] R. Tarroni and S. Carter, J. Chem. Phys. **119**, 12878 (2003).

[53] W. B. Yan, C. B. Dane, D. Zeitz, J. L. Hall, and R. F. Curl, J. Mol. Spectrosc. **123**, 486 (1987).

[54] K. M. Ervint and W. C. Lineberger, J. Phys. Chem. **95**, 1167–1177 (1991).

[55] J. Zhou, E. Garand, and D. M. Neumark, J. Chem. Phys. **127**, 154320 (2007).

[56] T. R. Taylor, C. S. Xu, and D. M. Neumark, J. Chem. Phys. **108**, 10018 (1998).

[57] H. Linnartz, T. Motylewski, O. Vaizert, J. P. Maier, A. J. Apponi, M. C. McCarthy, C. A. Gottlieb, and P. Thaddeus, J. Mol. Spectrosc. **197**, 1 (1999).

[58] K. Morokuma, J. Chem. Phys. **55**, 1236 (1971).

[59] T. Zielger and A. Rauk, Theor. Chim. Acta **46**, 1 (1977).